Deterministic generation of a quantum-dot-confined triexciton and its radiative decay via three-photon cascade

E. R. Schmidgall,[1] I. Schwartz,[1] L. Gantz,[1,2] D. Cogan,[1] S. Raindel,[2] and D. Gershoni[1,*]

[1]*Department of Physics and the Solid State Institute, The Technion–Israel Institute of Technology, Haifa 32000, Israel*
[2]*Department of Electrical Engineering, The Technion–Israel Institute of Technology, Haifa 32000, Israel*

Semiconductor quantum dots (QDs) have potential applications in quantum information processing due to the fact that they are potential on-demand sources of single and entangled photons. Generation of polarization-entangled photon pairs was demonstrated using the biexciton-exciton radiative cascade. One obvious way to increase the number of quantum correlated photons that the QDs emit is to use higher-order multiexcitons, in particular, the triexciton. Towards achieving this goal, we first demonstrate deterministic generation of the QD-confined triexciton in a well-defined coherent state and then spectrally identify and directly measure a three-photon radiative cascade resulting from the sequential triexciton-biexciton-exciton radiative recombination.

Semiconductor quantum dots (QDs) confine charge carriers in three spatial dimensions. This confinement results in a discrete spectrum of energy levels and energetically sharp optical transitions between these levels. These "atomiclike" features, together with their compatibility with semiconductor-based microelectronics and optoelectronics, make QDs promising building blocks for future technologies involving quantum information processing (QIP) [1,2] which rely on single photon detectors, single photon emitters, and light-matter interactions involving single photons and single carriers. Devices that emit single and entangled photons on demand are typical examples of these potential applications [3–7]. QDs are known sources of polarization-entangled photon pairs resulting from the biexciton-exciton radiative cascade [5,8,9]. Using pulsed laser excitation, this entangled photon pair emission process can, in principle, be performed on demand [7]. Deterministic generation of higher-order multiexcitons is a conceptual way for increasing the number of quantum correlated photons that a single QD emits. Here, we study the neutral triexciton (XXX^0) which contains three electron-hole (e-h) pairs, as a candidate for achieving this goal.

First, we discuss the optical transitions from the QD-confined ground neutral triexciton states to various biexciton (XX^0) states. We then experimentally identify these optical transitions using photoluminescence (PL) and PL excitation (PLE) spectroscopy. We use this information to demonstrate deterministic triexciton generation using a sequence of three nondegenerate laser pulses. We conclude by using third-order intensity cross-correlation measurements to demonstrate a triexciton-biexciton-exciton radiative cascade.

While there are previous reports on radiative cascades from triexcitons in single QDs [10,11], these reports fell short of identifying the triexciton fine structure, let alone demonstrating its deterministic generation or a three-photon radiative cascade.

The QD-confined XXX^0 contains three electron-hole (e-h) pairs. The population of these carriers in their ground state can be approximately described as a pair of electrons and a pair of heavy holes occupying their respective ground energy level forming an antisymmetric spin configuration (a singlet).

In addition, there is one unpaired electron and heavy hole in their respective second energy level. It follows, therefore, that the triexciton fine structure fully resembles that of the exciton (X^0) [12–15] where the unpaired e-h exchange interaction fully removes the degeneracy between the four possible e-h spin configurations, as schematically described in Fig. 1(a). There are two "bright" triexciton states in which the e-h pair spins are antiparallel and two "dark" triexciton states in which the e-h pair spins are parallel. Similarly to the exciton case, the degeneracy between the "dark" and "bright" triexciton pairs is further removed by the anisotropic and short range e-h exchange interactions, as seen in Fig. 1(a).

Radiative recombination between the triexciton e-h pairs occurs only between pairs of antiparallel spin directions [16,17]. In addition to opposite spins, efficient recombination requires also a significant e-h spatial envelope wave-function overlap [16,17]. Therefore, recombination mainly occurs between e-h pairs belonging to the same respective energy levels [16,17].

The recombination of the e-h pair in the second level is therefore possible only from the "bright" triexciton states. As the exciton case, these recombinations give rise to two cross-rectilinearly polarized spectral lines which leave a ground-state biexciton in the QD [XX^0, Fig. 1(b)]. The ground-state biexciton continues to radiatively decay by a well-studied two-photon radiative cascade [5,19–24], potentially providing a source of pairs of entangled photons on demand [5,7–9,23]. A comprehensive review of two-photon radiative cascades in QDs is available in Ref. [25]. In the case of this second-level recombination (not studied here), the triexciton forms a direct three-photon radiative cascade.

However, both the "dark" and the "bright" triexciton states can recombine radiatively by annihilating a ground-level e-h pair. For a thermally populated ground triexciton state, these recombinations occur in about five out of six recombinations. In these cases, an excited biexciton is left in the QD, containing one e-h pair in their respective ground levels and one in their respective second energy levels. The excited e-h pair usually relaxes to their ground level by phonon emission [26–28] before radiative recombination occurs. Thus an indirect photon radiative cascade is formed, involving a phonon emission in addition to the three photons.

*dg@physics.technion.ac.il
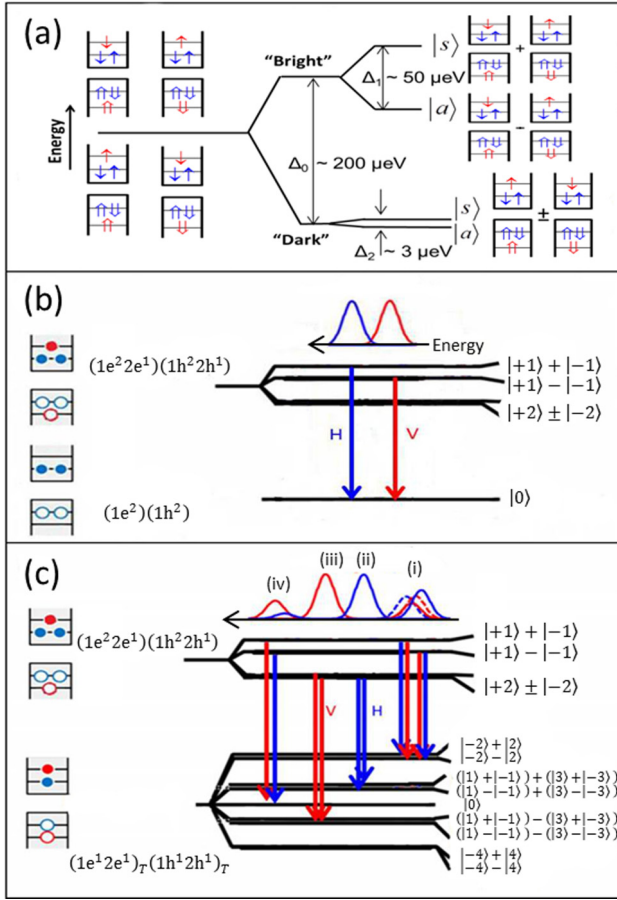
FIG. 1. (Color online) (a) Schematic illustration of the QD-confined ground-state triexciton. ↑ (⇑) represents an electron (heavy hole). The spin projection on the growth direction corresponds to the arrow direction. (b) [(c)] Allowed optical transitions from the triexciton states to the ground (excited e-triplet/h-triplet) biexciton state(s). Horizontal, H (vertical, V), rectilinearly polarized emission is indicated by blue (red) arrows. The total spin projection of the initial (final) state is presented to the right of the energy level. The calculated [18] PL emission spectrum (above the arrows) was obtained from a many-carrier model including direct and exchange Coulomb interactions between confined carriers. Allowed transitions and intensities were calculated using the dipole approximation [15].

There are $2^4 = 16$ possible spin configurations for the remaining carriers in the excited biexciton. These can be conveniently sorted in the following way, which takes into account same-carrier exchange interactions: one e-singlet/h-singlet state, three e-singlet/h-triplet states, three e-triplet/h-singlet states, and nine e-triplet/h-triplet states. All these states were observed in two-laser PLE spectroscopy [18]. Benny *et al.* [18] used the first laser pulse to generate an exciton in the QD and the second delayed, tunable pulse to search for excited biexciton absorption resonances. We used a similar technique, albeit with three laser pulses, to detect the direct "bright" triexciton optical transitions described in Fig. 1(b).

The optical transitions from the four triexciton states to the nine e-triplet/h-triplet excited biexciton states [Fig. 1(c)] are observed and identified here using polarization-sensitive PL spectroscopy. Transitions to biexciton states which involve same-carrier singlet configurations are more difficult to

observe in PL, since they rapidly decay nonradiatively to their ground singlet level. This rapid decay results in spectral broadening of the optical transitions to these states, thereby rendering their identification in PL spectroscopy quite challenging.

Figure 1(b) schematically illustrates the allowed optical transitions from the triexciton states to the ground biexciton state and, in Fig. 1(c), the optical transitions to the nine e-triplet/h-triplet states of the excited biexciton states. Horizontal (H) (vertical, V) polarized emission is indicated by blue (red) arrows. The total spin projection of the initial (final) state is presented to the right of the energy level. For example, $|+2\rangle$ corresponds to the normalized spin wave function of $|-1_e\rangle|+3_h\rangle$ where the electrons are in a spin-parallel down triplet state and the heavy holes are in a spin-parallel up triplet state. There are two allowed transitions to the ground biexciton state and ten allowed transitions to the excited triplet-triplet states. Taking into account the very small splitting between the "dark" triexciton states, the latter ten transitions yield three almost unpolarized transitions initiating from the "bright" triexciton states and two strongly rectilinearly polarized transitions initiating from the "dark" triexciton states. We note here the one-to-one correspondence between these triexciton-excited biexciton transitions and the exciton-excited biexciton transitions obtained in Ref. [18]. The calculated PL emission spectrum, from the many-carrier configuration-interaction (CI) model discussed in Ref. [18], is provided above the transition scheme. This model takes into account the direct and exchange Coulomb interactions between the quantum-confined carriers. We then use the dipole approximation to calculate the optical transitions between states for a given light polarization [15].

In general, the nine e-triplet/h-triplet excited biexciton states are spin blockaded from relaxation to the ground e-singlet/h-singlet biexciton state. There is, however, a relatively efficient spin flip-flop mechanism which permits this relaxation [28]. In this process, an electron and hole flip their spin mutually due to the enhanced effect of the e-h exchange interaction in the presence of a near resonant e-longitudinal optic (LO) phonon Frölich interaction [28]. The even (0 and ± 2) total spin excited biexciton states efficiently relax this way to the ground-state biexciton (XX^0), while the odd states (± 1 and ± 3) relax to the spin blockaded biexciton $XX^0_{T\pm3}$ states [27,29]. The relaxation to the $XX^0_{T\pm3}$ proceeds by emission of another photon and leaves the QD with a dark exciton [29,30]. The details of this two-photon radiative cascade are left for a forthcoming publication.

The sample used here was grown by molecular beam epitaxy (MBE) on a [001]-oriented GaAs substrate. One layer of self-assembled InGaAs QDs was deposited in the center of a one-wavelength planar microcavity designed for enhancing light harvesting resulting from emission due to a ground-level e-h recombination. As a result, however, detection of emission due to recombination of e-h pairs from the second level was practically eliminated. For optical measurements, the sample was placed inside a cryogenic tube, maintaining the sample temperature at 4 K. A 60×, 0.85 numerical aperture *in situ* microscope objective was used to focus the exciting laser lights on the sample surface and to collect the emitted PL light. For resonant pulse excitation three synchronously pumped energy-tunable dye lasers of 8 ps pulse width each and 76 MHz repetition rate were used. For nonresonant continuous wave
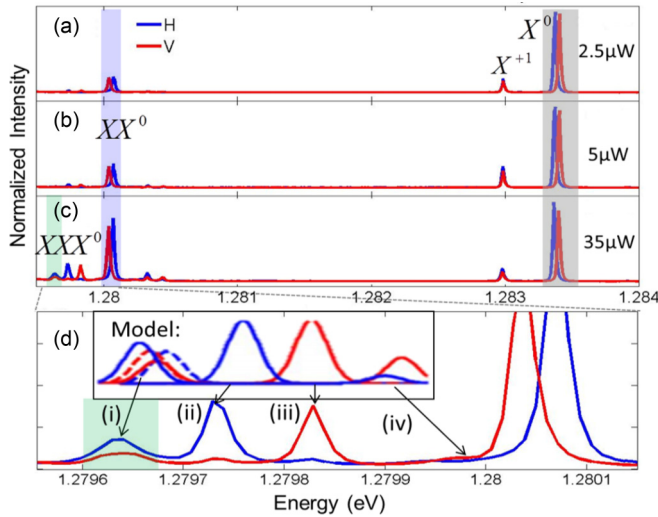
FIG. 2. (Color online) (a)–(c) Polarization-sensitive PL measurements for a single quantum dot under varying off-resonant excitation intensities. The initial state for recombination is indicated above each emission line. (d) The four triexcitonic emission lines compared with the calculated PL spectrum (inset). Roman numerals label the emission lines corresponding to the transitions in Fig. 1(c).

(cw) excitation, a 445 nm diode laser was used. The collected PL emission was split by a nonpolarizing beam splitter, and the polarization of the emitted light in each beam was analyzed using two computer-controlled liquid-crystal variable retarders and a polarizing beam splitter. The setup thus provided four PL collection channels. In each channel, the light was dispersed by a monochromator and detected by either a CCD camera or by a single-photon silicon avalanche photodetector. The setup provided a spectral resolution of about 15 μeV and a temporal resolution of about 400 ps.

Figure 2 presents polarization-sensitive PL spectra of the QD at increasing powers of the 445 nm light. At low excitation power, the dominant emission line is that corresponding to recombination from single excitons. Increasing excitation power results in increasing biexciton [Fig. 2(b)] and ultimately triexciton [Fig. 2(c)] PL emission. Figure 2(d) presents the measured triexciton emission next to the calculated spectrum [18]. Good correspondence is observed between the polarization-sensitive measurements and the calculated spectrum providing identification of the observed PL lines. The three shaded emission lines are the lines used for the third-order intensity correlation ($g^{(3)}$) measurements of the three-photon radiative cascade of the triexciton.

Potential use of the triexciton and its radiative cascade requires its deterministic generation in a well-defined spin configuration. Benny *et al.* [31] demonstrated a one-to-one correspondence between the polarization of a resonant laser pulse and the spin of the photogenerated bright exciton. Here, we use a sequence of three laser pulses to demonstrate the same ability for the bright triexciton. The first two π pulses deterministically generate the ground-state biexciton XX^0. A third, slightly delayed π pulse, resonantly tuned to the direct ground-state biexciton-bright triexciton transition [Fig. 1(b)], deterministically generates the triexciton.
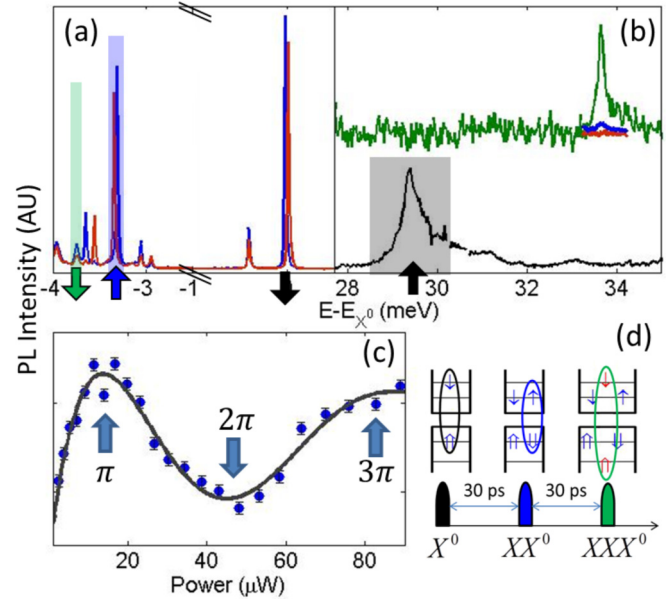
FIG. 3. (Color online) (a) Rectilinear polarization-sensitive PL spectra from a strongly excited QD. (b) The black (green) curve is the PLE spectrum of the X^0 (XXX^0) spectral line marked by a downward black (green) arrow in (a). The first (second) laser pulse is tuned to the X^0 (XX^0) absorption resonance indicated by the upward black (blue) arrow. The red (blue) curve is the PLE measurement in the absence of the first (second) pulse. (c) Measured (marks) XXX^0 PL intensity as a function of the average power of the third pulsed laser tuned to the resonance found in (b). The solid line describes a theoretical fit to the expected Rabi oscillation behavior. (d) Schematic description of the pulse sequence.

In Fig. 3(b), we present three-laser PLE measurements of one of the "bright" XXX^0 PL emission lines, indicated by a green arrow in the PL spectrum in Fig. 3(a) and corresponding to the emission line labeled (i) in Fig. 2(d). We used 30 ps interpulse temporal spacing between the three pulses, as shown in the schematic in Fig. 3(d). The first pulse is resonantly tuned to an excitonic absorption resonance at ~29 meV above the X^0 emission energy, corresponding to generation of a p-level electron and a s-level hole [18]. The electron relaxes quickly (~7 ps) to the X^0 state in a spin-preserving process [18,31]. The second pulse is resonantly tuned to the X^0-XX^0 transition energy. In Fig. 3(b), the solid green line shows the PL intensity from the XXX^0 emission line as a function of the energy of the third pulse. An absorption resonance is clearly visible ~34 meV above the exciton energy, corresponding to the addition of a p-level e-h pair to the XX^0 and the formation of XXX^0, as described in Fig. 1(b). The solid red (blue) line in Fig. 3(b) describes the same PLE measurement as that described by the green solid line but without the first (second) laser pulse, verifying that the triexciton PL indeed results only by the three pulses together. In Fig. 3(c), we present the XXX^0 PL intensity as a function of the average power of the third resonantly tuned pulse. Rabi oscillations are clearly visible, demonstrating that our three-pulse sequence deterministically photogenerates the triexciton. The polarization of the final pulse in the sequence determines the spin configuration of the unpaired p-level e-h pair [31]. Thus, the XXX^0 can be deterministically generated in any *a priori* well-defined spin configuration.

Intensity correlation measurements are the most common measurement technique to establish the quantum nature of light emitted from single photon sources, such as semiconductor QDs [32,33] and nanocrystals [34], and to characterize radiative cascades in QDs. In these cases,

$$g_{1,2}^{(2)}(\tau) = \langle I_1(t)I_2(t+\tau)\rangle / (\langle I_1(t)\rangle\langle I_2(t)\rangle)$$

is measured using a two-channel Hanbury Brown–Twiss (HBT) apparatus [19,20,25,35]. Here, $I_i(t)$ is the intensity of light at time t on the ith detector, τ is the time between the detection of a photon in detector 1 and detection of a subsequent photon in detector 2, and $\langle \rangle$ means temporal average. A radiative cascade is characterized by an asymmetric correlation function, due to the temporal order of the emitted photons. Following the detection of the second photon in a cascade, no detection of emission of the first photon is possible. Therefore "antibunching" [$g_{1,2}^{(2)}(\tau) < 1$] is anticipated. However, following the detection of the first photon, the probability of detecting the second photon is higher than the steady state probability [19,32] and bunching [$g_{1,2}^{(2)}(\tau) > 1$] is anticipated [19,20,25–27].

Here, for characterizing three-photon radiative cascades, we use a three-channel HBT apparatus for measuring the third-order intensity correlation function [36–40],

$$g_{1,2,3}^{(3)}(\tau_1,\tau_2) = \frac{\langle I_1(t)I_2(t+\tau_1)I_3(t+\tau_2)\rangle}{\langle I_1(t)\rangle\langle I_2(t)\rangle\langle I_3(t)\rangle}, \quad (1)$$

where τ_1 (τ_2) is the time between the detection of the first photon by the first detector and the time of detecting the second (third) photon by the second (third) detector. Using these definitions it is straightforward to show that

$$\left\langle g_{1,2,3}^{(3)}(\tau_1,\tau_2)\right\rangle_{\tau_2} = g_{1,2}^{(2)}(\tau_1),$$
$$\left\langle g_{1,2,3}^{(3)}(\tau_1,\tau_2)\right\rangle_{\tau_1} = g_{1,3}^{(2)}(\tau_2). \quad (2)$$

Figure 4(a) schematically describes the three-channel HBT system used to measure the third-order intensity correlation function. Detection times were recorded by a four-channel PicoQuant HydraHarp single-photon event timer [41]. Time differences between detection events on every channel were deduced and used to generate a multidimensional histogram. This way, three second-order [$g_{1,2}^{(2)}(\tau_{tb})$, $g_{1,3}^{(2)}(\tau_{te})$, $g_{2,3}^{(2)}(\tau_{be})$, where τ_{tb}, τ_{te} and $\tau_{be} = \tau_{te} - \tau_{tb}$ are the triexciton-biexciton, triexciton-exciton, and biexciton-exciton time differences, respectively] and one third-order [$g_{1,2,3}^{(3)}(\tau_{tb},\tau_{te})$] intensity correlation measurements were simultaneously carried out.

Figure 4 presents the measured intensity correlation functions for the three-photon radiative cascade initiating from the XXX^0. The first detector was tuned to the spectral line corresponding to a $|+1\rangle \pm |-1\rangle \rightarrow |2\rangle \pm |-2\rangle$ transition from XXX^0, the PL emission line labeled (i) in Fig. 2(d) and used for the PLE measurements in Fig. 3(b). The second and third detectors were tuned to the XX^0 emission line [blue shading in Figs. 2(a)–2(c)] and to the X^0 emission line [black shading in Figs. 2(a)–2(c)], respectively. Figure 4(b) shows a two-dimensional histogram (2D) displaying the number of three-photon events as a function of τ_{tb} and τ_{te}. The number of measured two-photon events in which only triexciton and biexciton (exciton) photons were detected are plotted as a
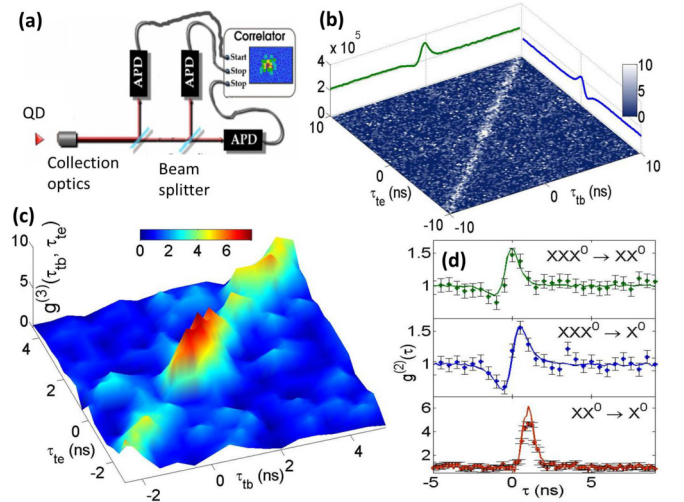
FIG. 4. (Color online) (a) Schematic description of the detection setup. (b) Histogram displaying the number of two-photon (edges) and three-photon (center) events as a function of τ_{tb} and τ_{te}. (c) 2D normalized histogram displaying the measured $g_{1,2,3}^{(3)}(\tau_{tb},\tau_{te})$, as deduced from (b). (d) The solid curves represent $g_{1,2}^{(2)}(\tau_{tb})$, $g_{1,3}^{(2)}(\tau_{te})$, and $g_{2,3}^{(2)}(\tau_{be})$ extracted from the corresponding two-photon events. The overlaid marks with error bars represent second-order intensity correlation functions extracted from the third-order intensity correlation function by temporal averaging [Eq. (2)].

function of $\tau_{tb}(\tau_{te})$ to the right (above) the 2D histogram in Fig. 4(b). We note the almost three orders of magnitude larger statistics accumulated for two-photon events than for three-photon events. Specifically, of the $\sim 3.4 \times 10^7$ recorded events, $\sim 99.95\%$ are two-photon events. There are a total of $\sim 16\,000$ recorded three-photon events in this data set. By comparing the number of recorded three-photon events with that of the two-photon events, one can directly obtain the light harvesting efficiency of the experimental setup. Assuming that all two-photon events result from triexciton radiative cascades, then the photon collection efficiency η_i of channel i is given by $\eta_i = N_{123}/N_{jk}$, where N_{123} (N_{jk}) is the total number of three- (two-) photon events (recorded in detectors j and k). The efficiencies of the three PL collection channels in our setup range from 1 in 600 to 1 in 1000.

In Fig. 4(c), we present the measured third-order intensity correlation function as obtained by normalizing the 2D histogram of Fig. 4(b). In Fig. 4(d), we present by solid lines three measured second-order intensity correlation functions as obtained by normalizing the large statistics one-dimensional (1D) histograms (from two-photon events) of Fig. 4(b). As a validity check of our approach, we obtained the second-order intensity correlation functions also by temporal summation over the measured third-order correlation function [Eq. (2)]. These data points are overlaid on the much higher statistics curves obtained from the measured two-photon events and the agreement is very good. Clearly, with higher statistics (e.g., by improving the light collection efficiency) these measurements could be applied for studying dynamical effects and coherence loss mechanisms which occur during the radiative cascades.

In conclusion, we have demonstrated deterministic generation of the QD-confined triexciton via a three-laser pulse sequence. We also identified and characterized the PL emission

lines due to all possible e-h recombinations from the ground states of the triexciton. Particularly, we investigated and conclusively characterized an indirect three-photon radiative cascade initiating from the triexciton using third-order intensity cross-correlation measurements. The experimental tools developed for characterization of multiphoton radiative cascades and higher-order excitonic states in semiconductor QDs are essential for further understanding many-carrier states in QDs and for protocols which require higher-order quantum correlations between carriers confined in these QDs and photons that they emit.

---

[1] A. Imamoḡlu, D. D. Awschalom, G. Burkard, D. P. DiVincenzo, D. Loss, M. Sherwin, and A. Small, Phys. Rev. Lett. **83**, 4204 (1999).

[2] D. Loss and D. P. DiVincenzo, Phys. Rev. A **57**, 120 (1998).

[3] C. Santori, M. Pelton, G. Solomon, Y. Dale, and Y. Yamamoto, Phys. Rev. Lett. **86**, 1502 (2001).

[4] Z. Yuan, B. E. Kardynal, R. M. Stevenson, A. J. Shields, C. J. Lobo, K. Cooper, N. S. Beattie, D. A. Ritchie, and M. Pepper, Science **295**, 102 (2001).

[5] N. Akopian, N. H. Lindner, E. Poem, Y. Berlatzky, J. Avron, D. Gershoni, B. D. Gerardot, and P. M. Petroff, Phys. Rev. Lett. **96**, 130501 (2006).

[6] A. Dousse, J. Suffczynski, A. Beveratos, O. Krebs, A. Lemaitre, I. Sagnes, J. Bloch, P. Voisin, and P. Senellart, Nature (London) **466**, 217 (2010).

[7] M. Muller, S. Bounouar, K. D. Jons, M. Glassl, and P. Michler, Nat. Photonics **8**, 224 (2014).

[8] R. J. Young, R. M. Stevenson, P. Atkinson, K. Cooper, D. A. Ritchie, and A. J. Shields, New J. Phys. **8**, 29 (2006).

[9] R. Hafenbrak, S. M. Ulrich, P. Michler, L. Wang, A. Rastelli, and O. G. Schmidt, New J. Phys. **9**, 315 (2007).

[10] Y. Arashida, Y. Ogawa, and F. Minami, Phys. Rev. B **84**, 125309 (2011).

[11] J. Persson, T. Aichele, V. Zwiller, L. Samuelson, and O. Benson, Phys. Rev. B **69**, 233314 (2004).

[12] M. Bayer, G. Ortner, O. Stern, A. Kuther, A. A. Gorbunov, A. Forchel, P. Hawrylak, S. Fafard, K. Hinzer, T. L. Reinecke, S. N. Walck, J. P. Reithmaier, F. Klopf, and F. Schäfer, Phys. Rev. B **65**, 195315 (2002).

[13] T. Takagahara, Phys. Rev. B **62**, 16840 (2000).

[14] E. L. Ivchenko and G. Pikus, *Superlattices and Other Heterostructures: Symmetry and Optical Phenomena*, Springer Series in Solid-State Sciences, 2nd ed. (Springer, Berlin, 1997).

[15] E. Poem, J. Shemesh, I. Marderfeld, D. Galushko, N. Akopian, D. Gershoni, B. D. Gerardot, A. Badolato, and P. M. Petroff, Phys. Rev. B **76**, 235304 (2007).

[16] G. Bastard, *Wave Mechanics Applied to Semiconductor Heterostructures*, 1st ed. (Wiley-Interscience, New York, 1991).

[17] L. Jacak, P. Hawrylak, and A. Wojs, *Quantum Dots* (Springer, Berlin, 1998).

[18] Y. Benny, Y. Kodriano, E. Poem, S. Khatsevitch, D. Gershoni, and P. M. Petroff, Phys. Rev. B **84**, 075473 (2011).

[19] D. V. Regelman, U. Mizrahi, D. Gershoni, E. Ehrenfreund, W. V. Schoenfeld, and P. M. Petroff, Phys. Rev. Lett. **87**, 257401 (2001).

[20] E. Moreau, I. Robert, L. Manin, V. Thierry-Mieg, J. M. Gérard, and I. Abram, Phys. Rev. Lett. **87**, 183601 (2001).

[21] A. Kiraz, S. Fälth, C. Becher, B. Gayral, W. V. Schoenfeld, P. M. Petroff, L. Zhang, E. Hu, and A. Imamoḡlu, Phys. Rev. B **65**, 161303(R) (2002).

[22] D. Gammon, E. S. Snow, B. V. Shanabrook, D. S. Katzer, and D. Park, Phys. Rev. Lett. **76**, 3005 (1996).

[23] O. Benson, C. Santori, M. Pelton, and Y. Yamamoto, Phys. Rev. Lett. **84**, 2513 (2000).

[24] V. D. Kulakovskii, G. Bacher, R. Weigand, T. Kümmell, A. Forchel, E. Borovitskaya, K. Leonardi, and D. Hommel, Phys. Rev. Lett. **82**, 1780 (1999).

[25] E. Poem and D. Gershoni, in *Handbook of Luminescent Semiconductor Materials*, edited by L. Bergman and J. L. McHalei (CRC, Boca Raton, FL, 2011).

[26] E. Poem, Y. Kodriano, C. Tradonsky, B. D. Gerardot, P. M. Petroff, and D. Gershoni, Phys. Rev. B **81**, 085306 (2010).

[27] Y. Kodriano, E. Poem, N. H. Lindner, C. Tradonsky, B. D. Gerardot, P. M. Petroff, J. E. Avron, and D. Gershoni, Phys. Rev. B **82**, 155329 (2010).

[28] Y. Benny, R. Presman, Y. Kodriano, E. Poem, D. Gershoni, T. A. Truong, and P. M. Petroff, Phys. Rev. B **89**, 035316 (2014).

[29] E. Poem, Y. Kodriano, C. Tradonsky, N. H. Lindner, B. D. Gerardot, P. M. Petroff, and D. Gershoni, Nat. Phys. **6**, 993 (2010).

[30] I. Schwartz, E. R. Schmidgall, L. Gantz, D. Cogan, E. Bordo, and D. Gershoni, arXiv:1408.2892.

[31] Y. Benny, S. Khatsevich, Y. Kodriano, E. Poem, R. Presman, D. Galushko, P. M. Petroff, and D. Gershoni, Phys. Rev. Lett. **106**, 040504 (2011).

[32] E. Dekel, D. Gershoni, E. Ehrenfreund, J. M. Garcia, and P. M. Petroff, Phys. Rev. B **61**, 11009 (2000).

[33] P. Michler, A. Kiraz, C. Becher, W. V. Schoenfeld, P. M. Petroff, Lidong Zhang, E. Hu, and A. Imamoglu, Science **290**, 2282 (2000).

[34] P. Michler, A. Imamoglu, M. D. Mason, P. J. Carson, G. F. Strouse, and S. K. Buratto, Nature (London) **406**, 968 (2000).

[35] R. Hanbury Brown and R. Q. Twiss, Nature (London) **177**, 27 (1956).

[36] R. J. Glauber, Phys. Rev. Lett. **10**, 84 (1963).

[37] M. Assmann, F. Veit, M. Bayer, M. van der Poel, and J. M. Hvam, Science **325**, 297 (2009).

[38] D. Elvira, X. Hachair, V. B. Verma, R. Braive, G. Beaudoin, I. Robert-Philip, I. Sagnes, B. Baek, S. W. Nam, E. A. Dauler, I. Abram, M. J. Stevens, and A. Beveratos, Phys. Rev. A **84**, 061802 (2011).

[39] M. J. Stevens, S. Glancy, S. W. Nam, and R. P. Mirin, Opt. Express **22**, 3244 (2014).

[40] A. Rundquist, M. Bajcsy, A. Majumdar, T. Sarmiento, K. Fischer, K. G. Lagoudakis, S. Buckley, A. Y. Piggott, and J. Vučković, Phys. Rev. A **90**, 023846 (2014).

[41] M. Wahl, H.-J. Rahn, I. Gregor, R. Erdmann, and J. Enderlein, Rev. Sci. Instrum. **78**, 033106 (2007).